Electronic Supplementary Information for Fault-Tolerant Computing with Single Qudit Encoding in a Molecular Spin

M. Mezzadri†,[1,2] A. Chiesa†,[1,2,3] L. Lepori,[1,2] and S. Carretta[1,2,3,*]

[1] *Università di Parma, Dipartimento di Scienze Matematiche, Fisiche e Informatiche, I-43124, Parma, Italy*
[2] *Gruppo Collegato di Parma, INFN-Sezione Milano-Bicocca, I-43124 Parma, Italy*
[3] *UdR Parma, INSTM, I-43124 Parma, Italy*

I. DERIVATION OF THE PULSE SEQUENCE

We now show how to derive the sequence of pulses to implement the various quantum computing operations (a.k.a. *gadgets*) described in the main text. The required connectivity (i.e. the possibility to drive transitions between pairs of levels involved in gates and correction), is achieved for both systems by employing x, y or z pulses resonant with the energy gap between two states. In addition, all pulses are assumed to be spectroscopically distinguishable, as reasonable for Molecular Nanomagnets, possibly with the help of suitable pulse-shaping techniques [1].

With these hypotheses and working in the basis of the eigenstates of the static system Hamiltonian $H_0 = \sum_{j=0}^{d-1} E_j \left|d_j\right\rangle \left\langle d_j\right|$, a set of simultaneous (circularly polarized) transverse pulses each addressing a different transition between a pair of qudit eigenstates can be described by the time-dependent Hamiltonian ($\hbar = 1$):

$$H_1(t) = \sum_{i<j} b_{ij} m_{ij} e^{-i(\omega_{ij} t + \phi_{ij})} \left|d_i\right\rangle \left\langle d_j\right| + \text{h.c.}. \tag{1}$$

Note that each amplitude b_{ij}, frequency ω_{ij} and phase ϕ_{ij} can be controlled independently, while m_{ij} is the system-dependent transition matrix element between the two eigenstates $|d_i\rangle$ and $|d_j\rangle$. In the case under investigation, this corresponds to the dipole magnetic moment parallel to the oscillating field. This *driving* Hamiltonian can be made time independent by moving to a generalized rotating frame [2], via the unitary transformation

$$U_{\text{rot}} = \sum_j e^{i\,\omega_{0j} t} \left|d_j\right\rangle \left\langle d_j\right| \tag{2}$$

where $\omega_{0,k} = \sum_{j=1}^{k} \omega_{j-1,j}$.

An analogous result is obtained starting with a linearly polarized pulse and omitting counter-rotating terms [3]. This leads to the generalized rotating frame Hamiltonian $H_{\text{rot}} = U_{\text{rot}}[H_1(t) + H_0]U_{\text{rot}}^{\dagger} - iU_{\text{rot}}\dot{U}_{\text{rot}}^{\dagger}$. H_{rot} takes the form:

$$H_{\text{rot}} = \sum_{i<j} \theta_{ij} e^{-i\varphi_{ij}} \left|d_i\right\rangle \left\langle d_j\right| + \text{h.c.} + \sum_{j=1}^{d-1} (E_j - \omega_{0j}) \left|d_j\right\rangle \left\langle d_j\right| \tag{3}$$

where $\theta_{ij} = b_{ij} m_{ij}$ and we have set $E_0 = 0$. The resulting time evolution can be computed in the generalized rotating frame as $e^{-iH_{\text{rot}} t}$. This shows that by choosing the set of ω_{ij} to be in resonance with the energy gaps in H_0 we selectively activate transitions between given pairs of eigenstates, while other states which are significantly off-resonance are not affected.

In practice this corresponds to the time evolution induced by an effective Hamiltonian $\tilde{H}$ with only some of the off diagonal terms activated at will, depending on the gadget that we aim to implement. This procedure can be realized in one shot with a single multi-frequency pulse and is the key to ensure Fault Tolerance. Below we show that each gadget can indeed be decomposed along these lines and recast into an effective zero-diagonal Hamiltonian $\tilde{H}$, corresponding to the different panels of Fig. 1 in the main text. Possible presence of diagonal terms in $\tilde{H}$ would require a slightly more complex pulse sequence.

* stefano.carretta@unipr.it

II. ERROR TRANSPARENT LOGICAL SINGLE-QUBIT ROTATIONS

We now describe a universal set of logical gates. First we recall that any unitary gate on a qudit can be decomposed (up to a global phase) into planar rotations (PRs) among any pair of levels [4–6], i.e.

$$R_{ij}^{P}(\theta,\varphi) \doteq \cos\frac{\theta}{2}\left(|d_i\rangle\langle d_i| + |d_j\rangle\langle d_j|\right) + \sin\frac{\theta}{2}\left(-e^{-i\varphi}|d_i\rangle\langle d_j| + e^{i\varphi}|d_j\rangle\langle d_i|\right). \tag{4}$$

Each PR can be implemented by a pulse resonant with the energy gap $E_j - E_i$, as discussed above. Indeed, it can be easily checked that $R_{ij}^{P}(\theta,\varphi) = \exp[-iH_{R^p}]$, with H_{R^p} in the $\{|d_i\rangle, |d_j\rangle\}$ subspace is given by

$$H_{R^p} = i\frac{\theta}{2}\begin{bmatrix} 0 & -e^{-i\varphi} \\ e^{i\varphi} & 0 \end{bmatrix} \tag{5}$$

which is exactly Eq. (3) restricted to a single pair of eigenstates in resonance.

Starting from this, we can easily construct a universal set of logical single-qubit gates from *logical planar rotations*:

$$R_L^p(\theta,\varphi) = R^p(\theta,\varphi)\otimes \mathrm{I}_{d/2} \tag{6}$$

The corresponding effective Hamiltonian in the rotating frame has the following simple form in the logical bases:

$$H_{R_L^p}^{(l)} = H_{R^p}\otimes \mathrm{I}_{d/2}. \tag{7}$$

To recover its form in the eigenbasis we perform the transformation

$$\tilde{H}_{R_L^p} = \mathcal{A} H_{R_L^p}^{(l)} \mathcal{A}^\dagger \tag{8}$$

where we recall that $\mathcal{A}$ is simply the set of code-words and error-words of the code. Thus imposing simple conditions on the structure on the elements of $\mathcal{A}$ we can ensure that $H_{R_L^p}$ has zero diagonal and hence it can be implemented by a set of simultaneous pulses. For example, if we set $d = 4$ and use the code words reported in Table S2 as in the main text, then

$$\tilde{H}_{R_L^p} = \begin{bmatrix} 0 & h_1 & h_2 & 0 \\ \bar{h}_1 & 0 & 0 & h_3 \\ \bar{h}_2 & 0 & 0 & h_4 \\ 0 & \bar{h}_3 & \bar{h}_4 & 0 \end{bmatrix}$$

III. ERROR TRANSPARENT TWO-QUBIT GATES

In the logical bases, a generic two-qubit controlled logical gates CG can be defined similarly to logical single-qubit rotations introduced in the main text. Let us suppose CG is written as

$$CG = \begin{bmatrix} \mathrm{G}_1 & 0 \\ 0 & \mathrm{G}_2 \end{bmatrix}$$

then the gate defined by

$$CG_L \doteq \begin{bmatrix} \mathrm{I}_{d/2}\otimes \mathrm{G}_1 \otimes \mathrm{I}_{d/2} & 0 \\ 0 & \mathrm{I}_{d/2}\otimes \mathrm{G}_2 \otimes \mathrm{I}_{d/2} \end{bmatrix} \tag{9}$$

is the logical representation of a controlled gate CG on two qubits, because it implements CG independently of the k of both the (logical) control and target. In our case we consider a logical $C{-}\varphi$, expressed in the logical two-qubit basis by the matrix

$$U_{C\text{-}\varphi} = \begin{bmatrix} 1 & 0 & 0 & 0 \\ 0 & 1 & 0 & 0 \\ 0 & 0 & 1 & 0 \\ 0 & 0 & 0 & e^{i\varphi} \end{bmatrix}.$$

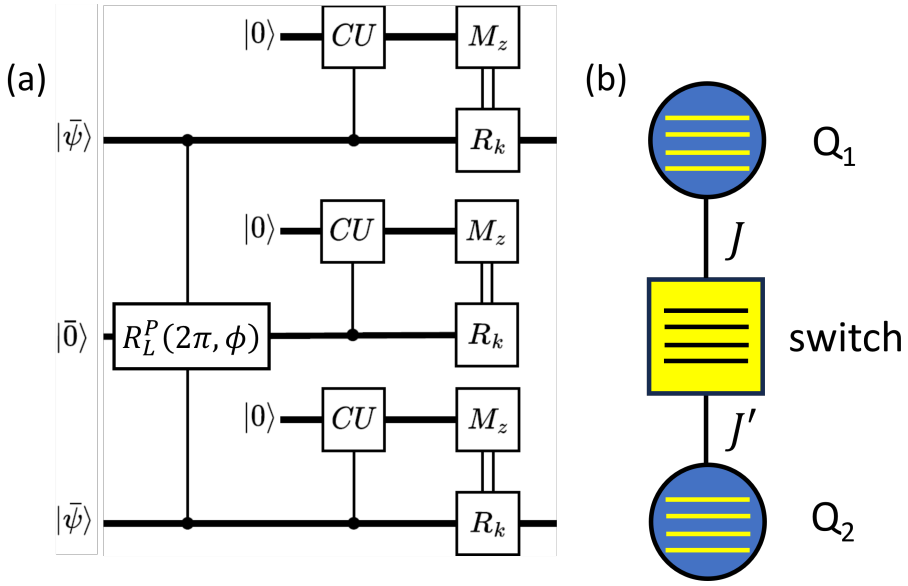

Figure S1: (a) Circuit for the implementation of a the Fault Tolerant two-qubit C-φ gate, followed by stabilization and measurement-dependent recovery. (b) Physical realization on a supra-molecular spin system consisting of three interacting spin qudits, where the middle one acts as a switch of the effective coupling between Q_1 and Q_2.

A. Implementation on molecular spins

Fig. S1-(a) reports the circuit for the FT implementation of the controlled-phase gate ($C-\varphi$) presented in the manuscript. To actually realize it on a real system, we consider the supra-molecule sketched in panel (b), consisting of three interacting logical qudits (LQs). They could be realized by three giant spin molecule, each one with $d^{(k)}=2S_k+1$. For them we can assume a leading interaction of the form

$$H_J=\sum_{i,i',i''=0}^{d-1}\left[J\left(\frac{d-1}{2}-i\right)\left(\frac{d-1}{2}-i'\right)+J'\left(\frac{d-1}{2}-i''\right)\left(\frac{d-1}{2}-i'''\right)\right]|d_i^{(1)}d_{i'}^{(Sw)}d_{i''}^{(2)}\rangle\langle d_i^{(1)}d_{i'}^{(Sw)}d_{i''}^{(2)}| \quad (10)$$

which could arise from a generic spin-spin exchange interaction between the qudits. Here $|d_i^{(1)}d_{i'}^{(S)}d_{i''}^{(2)}\rangle$ is the three-qudit $Q_1-\text{Switch}-Q_2$ state. From Eq. (10) we note that the energy needed to induce a *logical excitation of* the switch depends on the *logical state* of both Q_1 and Q_2. This naturally arises from the definition of logical state $\ell=0,1$ on two disjoint subspaces [7].

We now clarify how a conditional phase on Q_1, Q_2 can be obtained. The computational states of the the two LQs Q_1 and Q_2 are defined in the subspace in which the switch is in $|\bar{0}\rangle$. The excited logical state of the switch $|\bar{1}\rangle$ is only exploited to implement the $C-\varphi$. In particular, a resonant rotation of the switch $R_L^P(2\pi,\phi)$ (i.e. $|\bar{0}\rangle\rightarrow|\bar{1}\rangle\rightarrow|\bar{0}\rangle$) yields a phase π on the component of the wave-function which is excited. Since such a rotation is implemented only for a specific ($|\bar{1}\bar{1}\rangle$) state of Q_1 and Q_2, this becomes a conditional phase into the computational subspace.

In a similar way, a generic phase $\varphi\neq\pi$ can be obtained if one implements a semi-resonant rotation of the switch, which corresponds to a pulse slightly detuned from the addressed energy gap, where the detuning controls the phase φ [5, 8].

The FT implementation of the C-φ gate follows immediately the connectivity in the two-qubit bases, which follows from the all-to-all connectivity of each unit. Indeed, also this gate can be obtained starting from the zero-diagonal effective driving Hamiltonian $\tilde{H}_{C\varphi}$.

IV. STABILIZATION AND CORRECTION

We now turn our attention to the Fault Tolerant implementation of the stabilization process. Again, it turns out that the crucial requirement is the capability to directly implement planar rotations between any pair of qudit-ancilla eigenstates, i.e. to derive $\tilde{H}$ for this process.

As reported in the manuscript, to detect an error k we propose a k-controlled operation CU between the logical qubit and an ancilla with $d/2$ levels initialized in $|0\rangle$. Such a controlled excitation can be realized by considering two qudits interacting with a Hamiltonian of the form (10).

As an example, we set $d = 4$ and show the logical representation of the CU gate

$$\begin{bmatrix} 1 & 0 & 0 & 0 & 0 & 0 & 0 & 0 \\ 0 & 1 & 0 & 0 & 0 & 0 & 0 & 0 \\ 0 & 0 & 0 & -1 & 0 & 0 & 0 & 0 \\ 0 & 0 & 1 & 0 & 0 & 0 & 0 & 0 \\ 0 & 0 & 0 & 0 & 1 & 0 & 0 & 0 \\ 0 & 0 & 0 & 0 & 0 & 1 & 0 & 0 \\ 0 & 0 & 0 & 0 & 0 & 0 & 0 & -1 \\ 0 & 0 & 0 & 0 & 0 & 0 & 1 & 0 \end{bmatrix} \tag{11}$$

while in panel (d) of Fig. 1 (main text) its schematized implementation in the eigenbasis.

In the same setting, the two recovery operators have the following logical representations

$$R_0 = \begin{bmatrix} 1 & 0 & 0 & 0 \\ 0 & 1 & 0 & 0 \\ 0 & 0 & 1 & 0 \\ 0 & 0 & 0 & 1 \end{bmatrix} \tag{12}$$

$$R_1 = \begin{bmatrix} 0 & 1 & 0 & 0 \\ -1 & 0 & 0 & 0 \\ 0 & 0 & 0 & 1 \\ 0 & 0 & -1 & 0 \end{bmatrix} \tag{13}$$

and in panel (e) of Figure 1 (main text) is schematized the direct implementation of R_1 on the physical system.

V. NUMERICAL SIMULATIONS

A. Spin Hamiltonian of molecule 2

In the simulations for system **2** we have considered the illustrative 7-spin molecule introduced in Refs. [5, 9]. It is characterized by the following Hamiltonian:

$$H_1 = \sum_{i>j} J_{i,j} \mathbf{s}_i \cdot \mathbf{s}_j + \sum_{i>j} G_{i,j} (\mathbf{s}_i \times \mathbf{s}_j)_z + \mu_B B \sum_i g_i s_i^z, \tag{14}$$

where s_i^α are spin operators on sites $i = 1, ..., 7$, arranged to form a pair of corner-sharing tetrahedra as in the existing Ni_7 molecule [10]. In this molecule, the central spin is $s_7 = 3/2$, while all the others are $s_i = 1/2$. In Hamiltonian (14), the first term is the dominant Heisenberg exchange interaction between neighboring spin pairs with anti-ferromagnetic couplings $J_{i,j}$, the second is the (axial) anti-symmetric exchange coupling and the third is the Zeeman interaction with an external magnetic field B along z. By proper choice of the hierarchy between the different parameters, this Hamiltonian gives rise to an energy spectrum consisting of eight low-energy total spin 1/2 doublets well separated from the first excited $S = 3/2$. Due to the competition between anti-ferromagnetic exchange interactions in the spin Hamiltonian, the resulting situation is similar to spin frustration [11], with degeneracy of the ground state removed by slightly different values of $J_{i,j}$ and g_i, as typically occurs in real molecules [10, 12–19]. Moreover, the anti-symmetric exchange couples to first order all the different low-energy multiplets. *Hence, this molecule provides up to 16 low-energy eigenstates whose mutual transitions can be individually and directly addressed by resonant microwave pulses.* This feature is specifically exploited in the FT implementation of our protocol.

The parameters of such spin Hamiltonian are listed in the caption of Figure S2. The anti-ferromagnetic exchange couplings $J_{i,j}$, similar in magnitude and arranged as in Figure S2, give rise to a low-energy spectrum displaying several multiplets with total spin $S = 1/2$. The perturbative DMI term (combined with non-uniform g_i) then mixes these multiplets, giving rise to the all-to-all connectivity required by the scheme. We finally note that in **2** slight differences between the couplings in the spin Hamiltonian (typically occurring in real molecules with competing exchange interactions [12, 14–18]) ensure that all the energy gaps are distinguishable and hence can be individually addressed by resonant pulses.

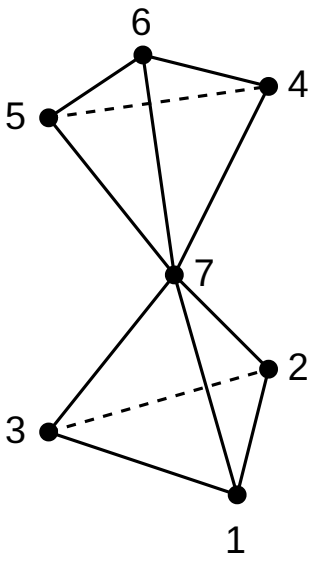

Figure S2: Magnetic structure of the representative 7-spin molecule considered in this work. Circles indicate magnetic ions (with $s_i = 1/2$ for $i = 1, ..., 7$ as for Cu^{2+} and $s_7 = 3/2$, as for Cr^{3+}), while bonds correspond to spin-spin interactions in the spin Hamiltonian (isotropic and anti-symmetric exchange). In the simulations, we have assumed $J_{1,2} = 1.14$ meV, $J_{1,3} = J_{2,3} = 1.15$ meV, $J_{4,5} = 1.13$ meV, $J_{4,6} = J_{5,6} = 1.10$ meV, $J_{1,7} = 0.82$ meV, $J_{2,7} = 0.85$ meV, $J_{3,7} = 0.87$ meV, $J_{4,7} = 0.83$ meV, $J_{5,7} = 0.81$ meV, $J_{6,7} = 0.90$ meV, $D_{i,j} = J_{i,j}/10$ and $g_i = (1.95, 2.032.05, 2.00, 1.98, 1.96, 2.06)$ for $i = 1, \ldots, 7$. Decoherence is ruled by a random distribution of surrounding nuclear spins, as described in Ref. [9]. The structure reproduces that of the existing Ni_7[10] cluster.

Note that for sake of simplicity we have assumed axial symmetry in the spin Hamiltonian. This choice does not qualitatively change our conclusions, but it affects the values of the transition matrix elements and hence the duration of the elementary transitions. Indeed, the duration of each transition is proportional to the product of the amplitude of the driving field and the matrix element of the magnetic dipole parallel to it. In our system, this yields 180 ns to perform the slowest π rotation between a couple of levels, setting a maximum amplitude for the driving field at 20 mT. Therefore, as a conservative assumption, we have chosen to set the duration of each operation in the QEC protocol to $\tau = 90$ ns, which corresponds to the slowest logical operation among those in the considered universal set. With parameters of the Hamiltonian of system **1** given in the main text we get comparable duration for the slowest π rotation. Hence, we fixed again $\tau = 90$ ns for the duration of the operations of the QEC protocol, corresponding to a maximum amplitude for the driving field of ~ 18 mT.

B. Lindblad equation for pure dephasing

Time evolution of the system is described in the Lindblad approximation, by considering the interaction of the system with a markovian nuclear spin bath. Although more accurate descriptions of the bath dynamics would be possible given a set of nuclear spin coordinates [20], this does not qualitatively affect our results. Hence, we prefer to adopt a simplified and more general picture, regardless of the specific molecular structure, following Refs. [5, 9]. Within this framework, the dynamics of the system is computed by solving the quantum master equation

$$\dot{\rho} = -i[H_{rot}, \rho] + \underbrace{\sum_{n,m} \frac{\Gamma_{n,m}}{T_2} \left(2 \left|d_n\right\rangle \left\langle d_n\right| \rho \left|d_m\right\rangle \left\langle d_m\right| - \delta_{n,m} \left|d_n\right\rangle \left\langle d_n\right| \rho - \delta_{n,m} \rho \left|d_m\right\rangle \left\langle d_m\right|\right)}_{D(\rho)} \tag{15}$$

and hence the differential equation is time independent and Γ_{mn} are system-specific dephasing rates. Switching to the superoperator formalism [21] [$H_{rot} \to \mathcal{H}$, $D \to \mathcal{D}$] we can rewrite (15) as

$$\frac{\partial}{\partial t} \left|\rho\right\rangle = \underbrace{\left[-i\mathcal{H} + \mathcal{D}\right]}_{\mathcal{F}[H]} \left|\rho\right\rangle$$

which has as a solution

$$\left|\rho\right\rangle (t) = e^{\mathcal{F}[H]t} \left|\rho\right\rangle (0).$$

In Eq. (15), $|d_n\rangle$ are system eigenstates and the dissipator term $D(\rho)$ induces a decay of each off-diagonal element

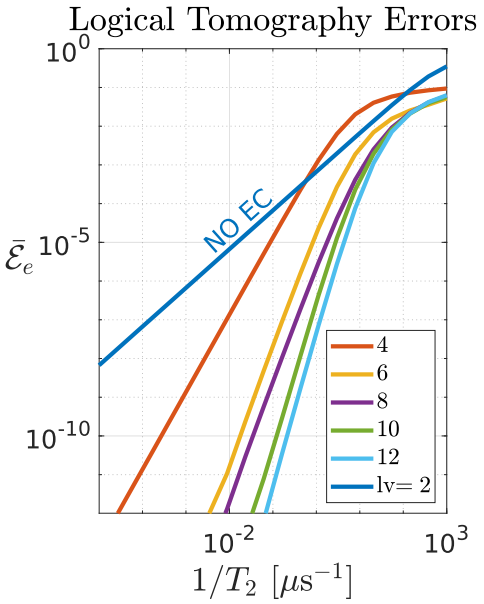

Figure S3: Simulation of the Fault-Tolerant implementation of single qubit logical gates on system **2**. Error $\mathcal{E}_e = 1 - \mathcal{F}_e^2$ as a function of $1/T_2$, where $\mathcal{F}_e$ is the entanglement fidelity [22], averaged over different planar rotations $R_L^p(\theta,\varphi)$ for $(\theta,\phi) = (\frac{\pi}{4},\pi),(\frac{\pi}{2},\pi),(\frac{\pi}{2},-\frac{\pi}{2}),(\frac{\pi}{2},-\frac{\pi}{4}),(\frac{\pi}{2},-\frac{\pi}{8})$.

ρ_{mn} of ρ with a rate $\gamma_{mn} = \Gamma_{mm} + \Gamma_{nn} - 2\Gamma_{mn}$. The Γ_{mn} coefficients are given by:

$$\Gamma_{mn} = \sum_{jj'=1}^{N} C_{jj'}^{zz} \langle d_m|s_j^z|d_m\rangle\langle d_n|s_{j'}^z|d_n\rangle, \tag{16}$$

where $C_{jj'}^{zz}$ depends on the molecular structure via the dipolar couplings between local system operators s_j^α and bath spin operators [9]. Note that here for both systems **1** and **2** (due to the form of the Hamiltonian) only $\alpha = z$ operators contribute, but the extension to a more general case would be straightforward. For the simulations reported in the text we have introduced the effective dephasing time $T_2 = \left(\sum_{jj'} C_{jj'}^{zz}\right)^{-1}$, which includes information on the bath.

The matrix elements of local spin operators in system **1** are proportional to the giant spin operators within the ground multiplet, i.e. $\langle d_i|\, s_k^z\, |d_i\rangle \propto \langle d_i|\, S_z\, |d_i\rangle$. Hence, $\Gamma_{m,n} = \langle d_m|\, S_z\, |d_m\rangle\, \langle d_n|\, S_z\, |d_n\rangle$. For **1** the Kraus operators describing the pure dephasing channel identified by the matrix Γ, and used to set the Knill-Laflamme conditions, are reported in Table S1. Moreover, code words and error words used in the simulations of the manuscript are reported in the Table S2. Conversely, in Table S3 and S4 are reported those for system **2**. Lastly, Fig. S3 is a zoom of the inset of Figure 2-(a) of the main text, where we report the performance of the code on system **2**.

We finally note that molecular spin qudits can be integrated within superconducting resonators which can be used to readout the final state of the system and to mediate the interaction between different qudits or clusters of qudits, thus enabling to entangle different parts of the register in a scalable architecture [6].

VI. MEASUREMENTS ERRORS

Ideal measurements on the $d/2-$levels ancilla are described by the projectors $P_k = |k\rangle\langle k|$. We model measurement errors at the end of the stabilization procedure by considering a deformation of the ideal projectors P_k as follows:

$$\Pi_k = (1-p)\,|k\rangle\langle k| + \frac{2p}{d-2}\sum_{j\neq k}|j\rangle\langle j|\,.$$

Π_k represent a simple generalization to qudits of the "measurement operators" introduced in Refs. [23, 24]. This gives a probability $2p/(d-2)$ of being projected onto each eigenstate $|j\neq k\rangle$, given k as the measurement output. A different choice in the distribution of the "wrong projectors" does not alter our conclusions. For instance, by assuming a probability of being projected onto $|j\rangle$ which decreases with $|j-k|$, we find an even smaller impact of the measurement error.

We first note that the recovery operation following a measurement error does not affect the state of the qudit. Indeed, suppose to have as measurement outcome k and to be projected onto $|j\neq k\rangle$. Then the qudit+ancilla state will be $(\alpha\,|0,j\rangle + \beta\,|1,j\rangle)\otimes|j\rangle$ and the recovery step R_k will be ineffective.

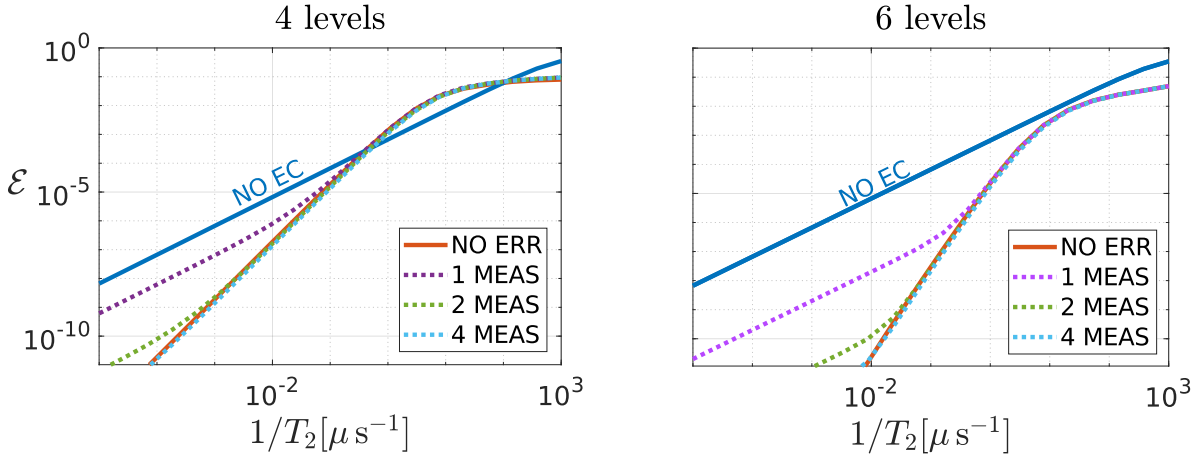

Figure S4: Comparison of the code performance with a measurement error probability $p = 0.01$ for system **1** and a qudit with 4 and 6 levels respectively. Dotted lines of different colors are obtained with $n = 1, 2, 4$ measurement repetitions, while continuous lines correspond to the case with no measurement errors (red) or no correction (blue). Clearly, measurement errors become negligible with a few measurement repetitions.

Hence, the measurement error can be suppressed by repeated measures of the ancilla, without needing to repeat the stabilization protocol [25]. In fact, after n repetitions, the measurement error probability $\sim p^n$ and hence can be made smaller than the error which is corrected by the code.

In Figure S4 we report simulations of the FT error-correction procedure for system **2**, including a measurement error with $p = 0.01$. We note that after a few repetitions of the measurement at the end of the protocol we can reduce $\mathcal{E}$ to an arbitrary extent, thus recovering the performance of the code with ideal measurements.

[1] A. Castro, A. García Carrizo, S. Roca, D. Zueco, and F. Luis, Phys. Rev. Appl. **17**, 064028 (2022).
[2] M. N. Leuenberger and D. Loss, Phys. Rev. B **68**, 165317 (2003).
[3] M. Kälin, I. Gromov, and A. Schweiger, J. Magn. Res. **160**, 166 (2003).
[4] G. K. Brennen, D. P. O'Leary, and S. S. Bullock, Phys. Rev. A **71**, 052318 (2005).
[5] M. Chizzini, L. Crippa, A. Chiesa, F. Tacchino, F. Petiziol, I. Tavernelli, P. Santini, and S. Carretta, Phys. Rev. Res. **4**, 043135 (2022).
[6] A. Chiesa, S. Roca, S. Chicco, M. de Ory, A. Gómez-León, A. Gomez, D. Zueco, F. Luis, and S. Carretta, Phys. Rev. Appl. **19**, 064060 (2023).
[7] A. Chiesa, F. Petiziol, E. Macaluso, S. Wimberger, P. Santini, and S. Carretta, AIP Adv. **11**, 025134 (2021).
[8] A. Chiesa, P. Santini, D. Gerace, J. Raftery, A. A. Houck, and S. Carretta, Sci. Rep. **5**, 16036 (2015).
[9] A. Chiesa, F. Petiziol, M. Chizzini, P. Santini, and S. Carretta, J. Phys. Chem. Lett. **13**, 6468 (2022).
[10] E. Garlatti, S. Carretta, M. Affronte, E. C. Sañudo, G. Amoretti, and P. Santini, J. Phys.: Cond. Matt. **24**, 104006 (2012).
[11] J. Schnack, Dalton Trans. **39**, 4677 (2010).
[12] M. Antkowiak, P. Kozłowski, G. Kamieniarz, G. A. Timco, F. Tuna, and R. E. P. Winpenny, Phys. Rev. B **87**, 184430 (2013).
[13] J. van Slageren, P. Rosa, A. Caneschi, R. Sessoli, H. Casellas, Y. V. Rakitin, L. Cianchi, F. D. Giallo, G. Spina, A. Bino, A.-L. Barra, T. Guidi, S. Carretta, and R. Caciuffo, Phys. Rev. B **73**, 014422 (2006).
[14] M. Baker, G. Timco, S. Piligkos, J. Mathieson, H. Mutka, F. Tuna, P. Kozlowski, M. Antkowiak, T. Guidi, T. Gupta, H. Rath, R. Woolfson, G. Kamieniarz, R. Pritchard, H. Weihe, L. Cronin, G. Rajaraman, D. Collison, E. McInnes, and R. Winpenny, Proc. Natl. Acad. Sci. U.S.A. **109**, 19113 (2012).
[15] W. Florek, M. Antkowiak, and G. Kamieniarz, Phys. Rev. B **94**, 224421 (2016).
[16] Y. Furukawa, K. Kiuchi, K.-i. Kumagai, Y. Ajiro, Y. Narumi, M. Iwaki, K. Kindo, A. Bianchi, S. Carretta, P. Santini, F. Borsa, G. A. Timco, and R. E. P. Winpenny, Phys. Rev. B **79**, 134416 (2009).
[17] L. M. Baker and et al., Chem. A Eur. J. **22**, 1779 (2016).
[18] R. J. Woolfson, G. A. Timco, A. Chiesa, I. J. Vitorica-Yrezabal, F. Tuna, T. Guidi, E. Pavarini, P. Santini, S. Carretta, and R. E. P. Winpenny, Angew. Chem. Int. Ed. **55**, 8856 (2016).
[19] F. Adelnia, A. Chiesa, S. Bordignon, S. Carretta, A. Ghirri, A. Candini, C. Cervetti, M. Evangelisti, M. Affronte, I. Sheikin, R. Winpenny, G. Timco, F. Borsa, and A. Lascialfari, J. Chem. Phys. **143**, 244321 (2015).
[20] F. Petiziol, A. Chiesa, S. Wimberger, P. Santini, and S. Carretta, npj Quantum Inf. **7**, 133 (2021).

Kraus Operators													
S	E_k	$\|d_0\rangle\langle d_0\|$	$\|d_1\rangle\langle d_1\|$	$\|d_2\rangle\langle d_2\|$	$\|d_3\rangle\langle d_3\|$	$\|d_4\rangle\langle d_4\|$	$\|d_5\rangle\langle d_5\|$	$\|d_6\rangle\langle d_7\|$	$\|d_7\rangle\langle d_7\|$	$\|d_8\rangle\langle d_8\|$	$\|d_9\rangle\langle d_9\|$	$\|d_10\rangle\langle d_10\|$	$\|d_11\rangle\langle d_11\|$
3/2	E_0	9.9988e-01	9.9918e-01	9.9996e-01	9.9888e-01								
	E_1	1.5707e-02	4.0417e-02	-8.8440e-03	-4.7298e-02								
	E_2	-4.7091e-04	6.6400e-04	-7.4171e-04	5.4969e-04								
	E_3	8.2900e-06	-2.9673e-06	-6.8142e-06	1.4916e-06								
5/2	E_0	9.9990e-01	9.9999e-01	9.9912e-01	9.9857e-01	9.9434e-01	9.9400e-01						
	E_1	1.3845e-02	6.8330e-04	4.2015e-02	-5.3461e-02	1.0607e-01	-1.0925e-01						
	E_2	-3.1148e-03	-3.3121e-03	-1.8661e-03	-1.5382e-03	5.2081e-03	4.6764e-03						
	E_3	3.9860e-05	-1.3702e-05	1.2853e-04	-1.7291e-04	-6.1284e-05	7.9509e-05						
	E_4	1.4722e-06	2.8763e-06	-3.1630e-06	-2.1725e-06	4.7478e-07	5.1222e-07						
	E_5	0	0	0	0	0	0						
7/2	E_0	9.9818e-01	9.9845e-01	9.9404e-01	9.9424e-01	9.6577e-01	9.5100e-01	8.9567e-01	8.9287e-01				
	E_1	-2.9842e-02	-1.6304e-02	-9.9385e-02	9.5037e-02	-2.5911e-01	3.0871e-01	-4.3089e-01	4.4012e-01				
	E_2	5.2457e-02	5.3177e-02	4.4452e-02	4.8853e-02	-2.8714e-03	-1.3242e-02	-1.0968e-01	-9.4764e-02				
	E_3	8.8417e-04	-1.5394e-04	5.9143e-03	-8.2922e-03	1.1377e-02	-1.1130e-02	-8.2252e-03	9.6327e-03				
	E_4	7.2467e-04	7.7038e-04	2.2514e-04	4.7312e-04	-1.8018e-03	-1.7786e-03	5.9583e-04	7.9650e-04				
	E_5	-3.4355e-05	-1.5118e-05	-1.0196e-04	1.3951e-04	7.0422e-05	-6.3861e-05	-1.2559e-05	1.7919e-05				
	E_6	-3.4312e-06	-6.4727e-06	7.4387e-06	4.2274e-06	-1.3162e-06	-7.0161e-07	1.2323e-07	1.3242e-07				
	E_7	0	0	0	0	0	0	0	0				
9/2	E_0	-9.9035e-01	-9.9045e-01	-9.8762e-01	-9.8990e-01	-9.6284e-01	-9.3330e-01	-8.4291e-01	-8.2256e-01	-7.2276e-01	-7.1329e-01		
	E_1	-3.2428e-02	-2.7153e-02	-9.0439e-02	3.5120e-02	-2.5511e-01	3.5005e-01	-5.1838e-01	5.5335e-01	-6.1435e-01	6.4251e-01		
	E_2	1.3461e-01	1.3502e-01	1.2713e-01	1.3650e-01	7.4596e-02	4.5983e-02	-1.3903e-01	-1.2726e-01	-3.1205e-01	-2.7343e-01		
	E_3	2.2449e-03	1.0070e-03	1.5657e-02	-1.3597e-02	4.7557e-02	-6.5203e-02	3.3305e-02	-2.8123e-02	-5.1655e-02	5.9209e-02		
	E_4	-5.9708e-03	-6.0713e-03	-4.2963e-03	-6.5915e-03	5.4246e-03	7.1850e-03	1.8679e-02	1.3850e-02	-1.1948e-02	-1.0845e-02		
	E_5	-2.5630e-05	-1.1790e-04	9.4517e-04	-1.2043e-03	2.4393e-03	-2.3836e-03	-2.5060e-03	3.1586e-03	1.0101e-03	-1.3166e-03		
	E_6	-1.7835e-04	-1.8667e-04	-4.6381e-05	-2.3373e-04	5.4532e-04	4.7540e-04	-2.2669e-04	-3.0833e-04	6.6627e-05	9.3236e-05		
	E_7	-4.3188e-06	-1.5235e-06	-2.8762e-05	2.7391e-05	1.3123e-05	-6.0558e-06	-2.0361e-06	2.2848e-06	4.2195e-07	-5.2520e-07		
	E_8	5.1837e-06	-1.3980e-06	-2.3015e-06	-1.7316e-06	1.6785e-07	1.0585e-07	-1.7769e-09	-3.0087e-08	-5.5613e-10	6.1662e-09		
	E_9	4.2821e-07	-4.1449e-06	1.9860e-06	1.9665e-06	-1.4987e-07	-1.1236e-07	5.2310e-12	3.2171e-08	9.0458e-10	-6.6248e-09		
11/2	E_0	9.7265e-01	9.7260e-01	9.7246e-01	9.7141e-01	9.4008e-01	8.7714e-01	7.1402e-01	5.4170e-01	3.9782e-01	3.3754e-01	2.4234e-01	2.1139e-01
	E_1	-4.5937e-02	-4.4176e-02	-7.9649e-02	-1.9985e-02	-2.3658e-01	2.9504e-01	-4.8518e-01	7.2867e-01	-5.4834e-01	8.1892e-01	-4.7797e-01	7.4458e-01
	E_2	-2.1709e-01	-2.1758e-01	-2.0588e-01	-2.2342e-01	-1.0290e-01	-1.6772e-01	3.2308e-01	2.3610e-01	7.2271e-01	4.4637e-01	7.5935e-01	4.8766e-01
	E_3	9.6073e-04	2.9468e-03	-3.7233e-02	3.0092e-02	-2.0953e-01	3.2055e-01	-3.1058e-01	2.6472e-01	5.5106e-02	-7.9135e-02	3.0220e-01	-3.3636e-01
	E_4	6.7111e-02	6.7376e-02	6.0393e-02	7.0168e-02	-1.3384e-02	-1.3406e-02	-2.2815e-01	-2.1848e-01	-6.9095e-02	-4.8071e-02	1.9499e-01	2.0984e-01
	E_5	-5.8178e-03	-5.0418e-03	-2.0458e-02	5.6708e-03	-7.2325e-02	1.0769e-01	1.3952e-02	-3.5554e-02	8.9726e-02	-7.2740e-02	-7.6913e-02	7.2243e-02
	E_6	-1.3090e-02	-1.3142e-02	-1.1396e-02	-1.3507e-02	1.2635e-02	2.6195e-02	3.8520e-02	1.9171e-02	-5.2708e-02	-4.3513e-02	3.0139e-02	2.5194e-02
	E_7	3.5648e-04	1.8511e-04	3.5844e-03	-2.1707e-03	1.2931e-02	-1.4696e-02	-1.4272e-02	2.0469e-02	1.0992e-02	-2.0908e-02	-5.1035e-03	8.7731e-03
	E_8	2.0834e-03	2.1316e-03	9.8305e-04	2.6980e-03	-6.7394e-03	-3.9804e-03	2.4769e-03	2.1260e-03	-1.1776e-03	-1.5459e-03	4.5186e-04	5.2490e-04
	E_9	-5.4228e-06	6.8450e-06	-2.0331e-04	1.7216e-04	4.8705e-05	-1.6506e-05	-5.9137e-06	3.7609e-06	1.6793e-06	-2.0598e-06	-5.2556e-07	5.9049e-07
	E_{10}	5.0413e-07	-2.5268e-06	8.8955e-07	1.1764e-06	-3.6623e-08	-8.5805e-09	1.5037e-09	8.3704e-10	-2.4521e-10	-3.4889e-10	6.0748e-11	8.5207e-11
	E_{11}	0	0	0	0	0	0	0	0	0	0	0	0

Table S1: Kraus decomposition for the pure dephasing channel considered for the search of codewords for system **2**. The diagonal operators E_k are obtained by process tomography of a free evolution of the system. In each row the diagonal elements of E_k are reported, in the basis of the eigenstates (columns).

[21] K. Blum, *Density Matrix Theory and Applications* (Springer Berlin Heidelberg, 2012).
[22] E. Knill, R. Laflamme, R. Martinez, and C. Negrevergne, Phys. Rev. Lett. **86**, 5811 (2001).
[23] A. Kandala, A. Mezzacapo, K. Temme, M. Takita, M. Brink, J. M. Chow, and J. M. Gambetta, Nature **549**, 242–246 (2017).
[24] S. Barnett, *Quantum information*, Vol. 16 (Oxford University Press, 2009).
[25] A. G. Fowler, M. Mariantoni, J. M. Martinis, and A. N. Cleland, Phys. Rev. A **86**, 032324 (2012).

Codewords and Errorwords													
S	$\|\ell,k\rangle$	$\|d_0\rangle$	$\|d_1\rangle$	$\|d_2\rangle$	$\|d_3\rangle$	$\|d_4\rangle$	$\|d_5\rangle$	$\|d_6\rangle$	$\|d_7\rangle$	$\|d_8\rangle$	$\|d_9\rangle$	$\|d_10\rangle$	$\|d_11\rangle$
3/2	$\|0,0\rangle$	0	8.5335e-01	5.2135e-01	0								
	$\|0,1\rangle$	0	5.2135e-01	-8.5335e-01	0								
	$\|1,0\rangle$	9.2188e-01	0	0	3.8748e-01								
	$\|1,1\rangle$	-3.8748e-01	0	0	9.2188e-01								
5/2	$\|0,0\rangle$	0	8.6730e-01	4.8736e-01	0	0	1.0135e-01						
	$\|0,1\rangle$	0	-3.5270e-01	7.4532e-01	0	0	-5.6577e-01						
	$\|0,2\rangle$	0	-3.5127e-01	4.5495e-01	0	0	8.1831e-01						
	$\|1,0\rangle$	9.5163e-01	0	0	2.8743e-01	1.0852e-01	0						
	$\|1,1\rangle$	1.9924e-01	0	0	-8.4622e-01	4.9417e-01	0						
	$\|1,2\rangle$	-2.3388e-01	0	0	4.4865e-01	8.6256e-01	0						
7/2	$\|0,0\rangle$	0	9.3589e-01	3.4838e-01	0	0	4.9608e-02	1.6842e-02	0				
	$\|0,1\rangle$	0	2.6564e-01	-7.7686e-01	0	0	5.2233e-01	-2.3043e-01	0				
	$\|0,2\rangle$	0	1.6583e-01	-3.0968e-01	0	0	-7.7601e-01	-5.2384e-01	0				
	$\|0,3\rangle$	0	-1.6139e-01	4.2335e-01	0	0	3.5002e-01	-8.1989e-01	0				
	$\|1,0\rangle$	9.7463e-01	0	0	2.0861e-01	7.9230e-02	0	0	1.7359e-02				
	$\|1,1\rangle$	-1.2072e-01	0	0	7.6080e-01	-5.7741e-01	0	0	2.7057e-01				
	$\|1,2\rangle$	1.3493e-01	0	0	-3.0685e-01	-7.1823e-01	0	0	-6.0974e-01				
	$\|1,3\rangle$	1.3160e-01	0	0	-5.3246e-01	-3.8008e-01	0	0	7.4479e-01				
9/2	$\|0,0\rangle$	0	-9.7383e-01	-2.2672e-01	0	0	-1.4979e-02	-5.3506e-03	0	0	-1.8138e-03		
	$\|0,1\rangle$	0	1.9829e-01	-8.7330e-01	0	0	3.8415e-01	-1.9764e-01	0	0	1.0679e-01		
	$\|0,2\rangle$	0	6.5647e-02	-2.2009e-01	0	0	-6.9368e-01	-5.3740e-01	0	0	-4.2102e-01		
	$\|0,3\rangle$	0	-6.5108e-02	2.8396e-01	0	0	1.3245e-01	-7.4936e-01	0	0	5.7969e-01		
	$\|0,4\rangle$	0	-6.1559e-02	2.3850e-01	0	0	5.9454e-01	-3.3251e-01	0	0	-6.8941e-01		
	$\|1,0\rangle$	-9.8143e-01	0	0	-1.8811e-01	-3.7275e-02	0	0	-5.1906e-03	-1.5884e-03	0		
	$\|1,1\rangle$	-1.3080e-01	0	0	7.8615e-01	-5.5211e-01	0	0	2.3078e-01	-8.2270e-02	0		
	$\|1,2\rangle$	7.0671e-02	0	0	-2.2961e-01	-5.9067e-01	0	0	-7.0310e-01	-3.1471e-01	0		
	$\|1,3\rangle$	8.6311e-02	0	0	-4.1201e-01	-2.5492e-01	0	0	6.2747e-01	-6.0340e-01	0		
	$\|1,4\rangle$	-8.5158e-02	0	0	3.5229e-01	5.2906e-01	0	0	-2.4217e-01	-7.2807e-01	0		
11/2	$\|0,0\rangle$	0	9.8856e-01	1.5076e-01	0	0	4.3251e-03	1.2628e-03	0	0	2.4555e-04	9.5793e-05	0
	$\|0,1\rangle$	0	1.4088e-01	-9.3101e-01	0	0	2.8657e-01	-1.3848e-01	0	0	1.0513e-01	-3.1951e-02	0
	$\|0,2\rangle$	0	-2.5000e-02	1.4153e-01	0	0	5.8223e-01	5.6226e-01	0	0	5.1452e-01	2.4391e-01	0
	$\|0,3\rangle$	0	2.9559e-02	-1.9520e-01	0	0	-8.6152e-02	5.5448e-01	0	0	-6.6641e-01	4.4950e-01	0
	$\|0,4\rangle$	0	2.5039e-02	-1.4732e-01	0	0	-6.2127e-01	-2.7700e-02	0	0	4.9706e-01	5.8639e-01	0
	$\|0,5\rangle$	0	2.7839e-02	-1.7509e-01	0	0	-4.3066e-01	5.9705e-01	0	0	1.8180e-01	-6.2736e-01	0
	$\|1,0\rangle$	9.8069e-01	0	0	1.9520e-01	1.2284e-02	0	0	6.0336e-04	2.8044e-04	0	0	-8.4286e-05
	$\|1,1\rangle$	-1.6733e-01	0	0	8.6776e-01	-4.3699e-01	0	0	1.4538e-01	-6.4694e-02	0	0	-5.2088e-02
	$\|1,2\rangle$	-4.8225e-02	0	0	2.0262e-01	5.8952e-01	0	0	5.9506e-01	4.2155e-01	0	0	-2.7802e-01
	$\|1,3\rangle$	-5.1456e-02	0	0	2.4766e-01	1.8644e-01	0	0	-5.2764e-01	6.5223e-01	0	0	4.4435e-01
	$\|1,4\rangle$	5.5394e-02	0	0	-2.4499e-01	-5.4425e-01	0	0	-4.2385e-02	5.8775e-01	0	0	-5.4172e-01
	$\|1,6\rangle$	-4.7068e-02	0	0	2.1559e-01	3.6110e-01	0	0	-5.8700e-01	-2.1741e-01	0	0	-6.5504e-01

Table S2: Error-words set $\mathcal{A}$ used in the simulations (**2**) for different values of S

Kraus Operators													
d	E_k	$\|d_0\rangle\langle d_0\|$	$\|d_1\rangle\langle d_1\|$	$\|d_2\rangle\langle d_2\|$	$\|d_3\rangle\langle d_3\|$	$\|d_4\rangle\langle d_4\|$	$\|d_5\rangle\langle d_5\|$	$\|d_6\rangle\langle d_7\|$	$\|d_7\rangle\langle d_7\|$	$\|d_8\rangle\langle d_8\|$	$\|d_9\rangle\langle d_9\|$	$\|d_{10}\rangle\langle d_{10}\|$	$\|d_{11}\rangle\langle d_{11}\|$
4	E_0	9.5932e-1	9.5929e-1	9.9860e-1	9.9860e-1								
	E_1	-2.8077e-1	2.8087e-1	-4.4602e-2	4.4521e-2								
	E_2	2.9562e-2	2.9546e-2	-2.8384e-2	-2.8398e-2								
	E_3	-2.3623e-4	2.3594e-4	1.4879e-3	-1.4876e-3								
6	E_0	9.5950e-1	9.5950e-1	9.9835e-1	9.9836e-1	9.6435e-1	9.6429e-1						
	E_1	-2.8082e-1	2.8082e-1	-4.4659e-2	4.4469e-2	-2.6419e-1	2.6440e-1						
	E_2	2.2269e-2	2.2207e-2	-3.5994e-2	-3.6015e-2	1.5133e-2	1.5164e-2						
	E_3	-6.9188e-4	6.8550e-4	1.4152e-3	-1.4167e-3	4.9691e-4	-4.8910e-4						
	E_4	-7.2891e-5	-7.2905e-5	-1.0536e-5	-9.6752e-6	8.3099e-5	8.2893e-5						
	E_5	0	0	0	0	0	0						
8	E_0	9.5927e-1	9.5929e-1	9.9862e-1	9.9863e-1	9.6418e-1	9.6413e-1	9.9667e-1	9.9666e-1				
	E_1	-2.8084e-1	2.8079e-1	-4.4685e-2	4.4446e-2	-2.6421e-1	2.6438e-1	-7.7726e-2	7.7863e-2				
	E_2	-3.0497e-2	-3.0442e-2	2.7428e-2	2.7448e-2	-2.3402e-2	-2.3441e-2	2.4495e-2	2.4488e-2				
	E_3	-1.0181e-3	1.0119e-3	1.3661e-3	-1.3622e-3	1.9011e-4	-1.8169e-4	2.2479e-3	-2.2540e-3				
	E_4	-7.2707e-5	-7.1503e-5	-3.3964e-5	-3.7550e-5	8.1375e-5	7.9642e-5	2.5735e-5	2.8955e-5				
	E_5	6.0405e-6	-2.7071e-7	-1.1425e-5	-4.6362e-6	-7.7097e-6	9.8859e-8	1.2784e-5	5.1182e-6				
	E_6	-1.5229e-6	1.0861e-6	-3.5611e-6	4.4748e-6	1.8392e-6	-1.2773e-6	1.1968e-6	-2.2355e-6				
	E_7	0	0	0	0	0	0	0	0				
10	E_0	9.5910e-1	9.5913e-1	9.9874e-1	9.9876e-1	9.6405e-1	9.6402e-1	9.9678e-1	9.9677e-1	9.9605e-1	9.9603e-1		
	E_1	-2.8087e-1	2.8077e-1	-4.4712e-2	4.4422e-2	-2.6424e-1	2.6435e-1	-7.7755e-2	7.7841e-2	-8.6782e-2	8.6972e-2		
	E_2	-3.5125e-2	-3.5075e-2	2.2607e-2	2.2627e-2	-2.8054e-2	-2.8096e-2	1.9685e-2	1.9676e-2	1.8609e-2	1.8587e-2		
	E_3	-1.3832e-3	1.3774e-3	1.3091e-3	-1.3032e-3	-1.5319e-4	1.6259e-4	2.1478e-3	-2.1517e-3	2.3440e-3	-2.3497e-3		
	E_4	-7.2727e-5	-7.1423e-5	-5.1930e-5	-5.4520e-5	7.9499e-5	7.7658e-5	8.5971e-6	1.2331e-5	3.6789e-5	3.5706e-5		
	E_5	5.7772e-6	-1.5996e-6	-8.3151e-6	-5.9987e-6	-7.3003e-6	1.7634e-6	1.3993e-5	7.9634e-6	-3.3723e-6	-2.9114e-6		
	E_6	4.6381e-7	-3.7427e-6	8.1755e-6	-2.8211e-6	-3.9084e-7	4.7019e-6	-4.5037e-6	8.1123e-6	-1.2281e-6	-8.7672e-6		
	E_7	0	0	0	0	0	0	0	0	0	0		
	E_8	0	0	0	0	0	0	0	0	0	0		
	E_9	0	0	0	0	0	0	0	0	0	0		
12	E_0	9.5901e-1	9.5904e-1	9.9880e-1	9.9881e-1	9.6397e-1	9.6394e-1	9.9682e-1	9.9682e-1	9.9610e-1	9.9608e-1	9.9376e-1	9.9376e-1
	E_1	-2.8087e-1	2.8076e-1	-4.4716e-2	4.4423e-2	-2.6424e-1	2.6435e-1	-7.7760e-2	7.7843e-2	-8.6787e-2	8.6974e-2	-1.1082e-1	1.1083e-1
	E_2	-3.7608e-2	-3.7559e-2	2.0021e-2	2.0040e-2	-3.0550e-2	-3.0593e-2	1.7103e-2	1.7095e-2	1.6029e-2	1.6007e-2	1.2586e-2	1.2585e-2
	E_3	-1.8724e-3	1.8665e-3	1.2315e-3	-1.2257e-3	-6.1333e-4	6.2308e-4	2.0126e-3	-2.0159e-3	2.1930e-3	-2.1980e-3	2.5812e-3	-2.5826e-3
	E_4	-7.6383e-5	-7.4853e-5	-7.6873e-5	-7.8148e-5	7.5222e-5	7.3132e-5	-1.4054e-5	-1.1373e-5	1.2387e-5	1.2181e-5	7.9604e-5	7.9129e-5
	E_5	-6.1490e-6	1.4332e-6	7.9624e-6	6.3313e-6	7.6852e-6	-1.4298e-6	-1.5432e-5	-4.9528e-6	1.9022e-6	3.5333e-6	2.2768e-6	-3.1608e-6
	E_6	-4.6658e-7	3.3774e-6	-5.9841e-6	2.2090e-6	5.1232e-7	-4.3400e-6	3.8599e-6	-1.0805e-5	3.4255e-6	8.2307e-6	-2.5374e-6	2.5187e-6
	E_7	1.2549e-6	-1.6023e-6	4.8624e-6	-6.0655e-6	-1.3402e-6	1.8267e-6	-1.0629e-6	-1.1922e-6	4.6939e-6	1.9815e-6	-4.8245e-6	1.4683e-6
	E_8	-3.9082e-7	1.0772e-6	-1.4755e-6	-3.0191e-6	3.8496e-7	-1.2460e-6	-3.0864e-7	3.3828e-6	1.1338e-8	4.9039e-6	1.1633e-6	-4.4833e-6
	E_9	0	0	0	0	0	0	0	0	0	0	0	0
	E_{10}	0	0	0	0	0	0	0	0	0	0	0	0
	E_{11}	0	0	0	0	0	0	0	0	0	0	0	0

Table S3: Kraus decomposition for the pure dephasing channel considered for the search of codewords for system **1**. The diagonal operators E_k are obtained by process tomography of a free evolution of the system for $t/T_2 = 0.05$. In each row the diagonal elements of E_k are reported, in the basis of the eigenstates (columns).

Codewords and Errorwords													
d	$\|\ell,k\rangle$	$\|d_0\rangle$	$\|d_1\rangle$	$\|d_2\rangle$	$\|d_3\rangle$	$\|d_4\rangle$	$\|d_5\rangle$	$\|d_6\rangle$	$\|d_7\rangle$	$\|d_8\rangle$	$\|d_9\rangle$	$\|d_{10}\rangle$	$\|d_{11}\rangle$
4	$\|0,0\rangle$	-3.6381e-1	0	0	-9.3147e-1								
	$\|0,1\rangle$	9.3147e-1	0	0	-3.6381e-1								
	$\|1,0\rangle$	0	-3.6358e-1	-9.3156e-1	0								
	$\|1,1\rangle$	0	-9.3156e-1	3.6358e-1	0								
6	$\|0,0\rangle$	5.6039e-1	0	5.4604e-1	0	0	6.2274e-1						
	$\|0,1\rangle$	-6.9164e-1	0	-1.0512e-1	0	0	7.1455e-1						
	$\|0,2\rangle$	4.5564e-1	0	-8.3114e-1	0	0	3.1875e-1						
	$\|1,0\rangle$	0	5.6385e-1	0	5.4585e-1	6.1978e-1	0						
	$\|1,1\rangle$	0	6.9075e-1	0	9.9654e-2	-7.1619e-1	0						
	$\|1,2\rangle$	0	4.5269e-1	0	-8.3194e-1	3.2086e-1	0						
8	$\|0,0\rangle$	2.4417e-1	2.5358e-1	5.9709e-1	0	0	0	0	7.2080e-1				
	$\|0,1\rangle$	-6.6189e-1	5.7514e-1	-3.5925e-1	0	0	0	0	3.1947e-1				
	$\|0,2\rangle$	-6.3845e-1	-6.8064e-1	2.8324e-1	0	0	0	0	2.2110e-1				
	$\|0,3\rangle$	-3.0768e-1	3.7635e-1	6.5893e-1	0	0	0	0	-5.7402e-1				
	$\|1,0\rangle$	0	0	0	8.4196e-1	2.7220e-1	2.9993e-1	3.5646e-1	0				
	$\|1,1\rangle$	0	0	0	1.3247e-1	-6.9449e-1	6.3306e-1	-3.1523e-1	0				
	$\|1,2\rangle$	0	0	0	3.9018e-1	-6.0336e-1	-6.8574e-1	1.1611e-1	0				
	$\|1,3\rangle$	0	0	0	-3.4831e-1	-2.8204e-1	1.9759e-1	8.7183e-1	0				
10	$\|0,0\rangle$	0	1.7824e-1	6.4579e-1	0	2.1002e-1	0	3.4115e-1	0	0	6.2505e-1		
	$\|0,1\rangle$	0	5.0187e-1	-3.0401e-1	0	-5.6785e-1	0	-2.7101e-1	0	0	5.0970e-1		
	$\|0,2\rangle$	0	-6.6559e-1	2.7372e-1	0	-6.8361e-1	0	7.3945e-2	0	0	9.6338e-2		
	$\|0,3\rangle$	0	5.2096e-1	3.7730e-1	0	-4.0323e-1	0	3.1021e-1	0	0	-5.7221e-1		
	$\|0,4\rangle$	0	-4.4176e-2	-5.2273e-1	0	-5.9291e-2	0	8.4171e-1	0	0	1.1320e-1		
	$\|1,0\rangle$	1.7466e-1	0	0	6.3406e-1	0	2.1376e-1	0	4.0840e-1	5.9580e-1	0		
	$\|1,1\rangle$	-5.0413e-1	0	0	2.5254e-1	0	5.6334e-1	0	2.9635e-1	-5.2622e-1	0		
	$\|1,2\rangle$	-6.6169e-1	0	0	2.7450e-1	0	-6.8629e-1	0	9.3800e-2	8.3772e-2	0		
	$\|1,3\rangle$	-5.2433e-1	0	0	-3.2005e-1	0	4.0204e-1	0	-3.4362e-1	5.8561e-1	0		
	$\|1,4\rangle$	-5.0906e-2	0	0	-5.9700e-1	0	-6.5762e-2	0	7.8646e-1	1.3476e-1	0		
12	$\|0,0\rangle$	0	1.1937e-1	0	6.6218e-1	2.5044e-2	0	2.5382e-1	0	3.5742e-1	0	0	5.9538e-1
	$\|0,1\rangle$	0	3.8844e-1	0	-2.1066e-2	-1.0639e-1	0	-4.1952e-1	0	-6.3391e-1	0	0	5.0943e-1
	$\|0,2\rangle$	0	-7.8810e-1	0	4.1293e-1	-2.4141e-1	0	-1.8374e-1	0	-3.4100e-1	0	0	-8.0619e-3
	$\|0,3\rangle$	0	4.1871e-1	0	3.7430e-1	-6.8064e-1	0	5.5312e-2	0	-5.1394e-2	0	0	-4.6434e-1
	$\|0,4\rangle$	0	-1.9580e-1	0	-4.9610e-1	-6.8184e-1	0	1.3387e-1	0	2.5262e-1	0	0	4.1098e-1
	$\|0,5\rangle$	0	1.0829e-2	0	6.5901e-2	-3.9993e-2	0	-8.3955e-1	0	5.3635e-1	0	0	-3.7860e-2
	$\|1,0\rangle$	2.1515e-2	0	4.8120e-1	0	0	1.4807e-1	0	3.9098e-1	0	7.2870e-1	2.4937e-1	0
	$\|1,1\rangle$	-9.6743e-2	0	-5.8368e-1	0	0	4.4555e-1	0	1.6151e-1	0	3.8999e-1	-5.2275e-1	0
	$\|1,2\rangle$	-2.3512e-1	0	-1.7972e-2	0	0	-8.2968e-1	0	1.6647e-1	0	2.3956e-1	-4.1343e-1	0
	$\|1,3\rangle$	-6.9788e-1	0	4.9851e-1	0	0	2.9222e-1	0	-4.4245e-2	0	-2.2186e-1	-3.5758e-1	0
	$\|1,4\rangle$	-6.6511e-1	0	-4.0142e-1	0	0	-7.4867e-2	0	-1.2133e-1	0	1.6267e-1	5.9136e-1	0
	$\|1,5\rangle$	7.4011e-2	0	1.3336e-1	0	0	-1.3742e-2	0	-8.8128e-1	0	4.2875e-1	-1.2673e-1	0

Table S4: Error-words set $\mathcal{A}$ used in the simulations (**1**) for different qudit size d.